

Supporting Information

for

Molecular Tunnel Junctions Based on Mixed SAMs: Exponential Correlation of the Average Metal-HOMO Coupling with SAM/Metal Work Function

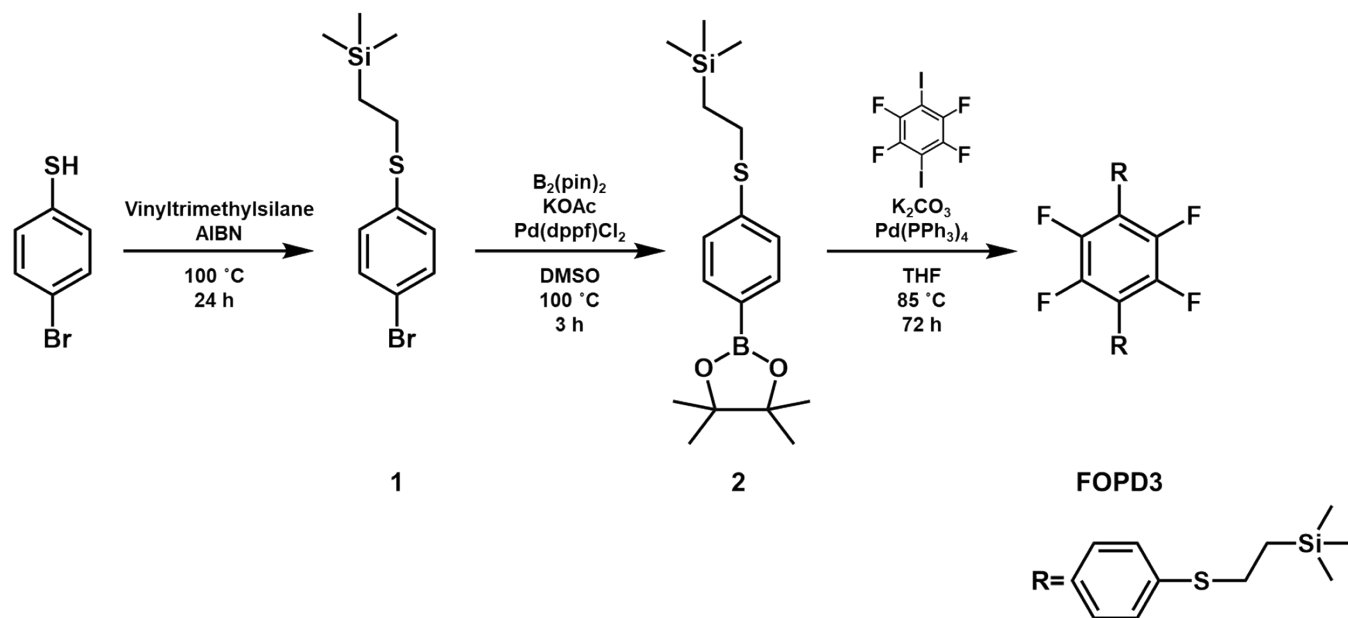
Gookyeong Jeong, C. Daniel Frisbie*

Department of Chemical Engineering and Materials Science, University of Minnesota,
Minneapolis, Minnesota 55455, United States

*E-mail: frisbie@umn.edu

1. Molecular Synthesis
2. X-ray Photoelectron Spectroscopy (XPS)
3. Angle Resolved XPS (ARXPS)
4. Ultraviolet Photoelectron Spectroscopy (UPS)
5. *I-V* traces for Ag Single Component Junctions
6. Fit to the Non-Dimensionalized Prediction for Off-Resonance Tunneling
7. Current-Voltage Behavior of Binary Component SAMs
8. Single Level Model Analysis with Mixed SAM Composition
9. Density Functional Calculations of HOMO for BOPD3, FOPD3, and OPD3

1. Molecular Synthesis



1.1 Synthesis of FOPD3 (2',3',5',6'-tetrafluoro-terphenyl dithiol)

Compound 1. To 20 mL of pressure tube was added 4-bromothiophenol (2 g, 10.58 mmol), vinyltrimethylsilane (2 mL, 13.65 mmol), and azobisisobutyronitrile (AIBN), (20 mg, 0.12 mmol). After 20 minutes purging with N_2 , it was heated with stirring at 100 °C for 24 h. It was cooled down to room temperature, diluted with DCM, and concentrated under reduced pressure. 3.0 g of compound 1 was obtained as yellow liquid (yield: 95%). The crude product was used for the next step without further purification.

Compound 2. Compound 1 (1 g, 3.46 mmol, 1 equiv.), bis(pinacolato)diboron (1.76 g, 6.93 mmol, 2 equiv.), potassium acetate (1.02 g, 10.37 mmol, 3 equiv.), and $\text{Pd}(\text{dppf})\text{Cl}_2$ (0.24 g, 0.33 mmol, 0.1 equiv.) were added in a 25 mL two-neck round bottom flask. 10 mL of 1,4-dioxane was added and it was purged with N_2 for 20 minutes. It was stirred under reflux condition for 3 h until all starting materials disappeared in TLC. Saturated NaCl solution was added to the solution,

and it was extracted with ethyl acetate 4 times. The organic solution was dried with sodium sulfate and concentrated under reduced pressure. The crude product was purified by column chromatography (Hexane : EA = 98 : 2), and 0.48 g of compound **2** was obtained as white solid (yield: 41%).

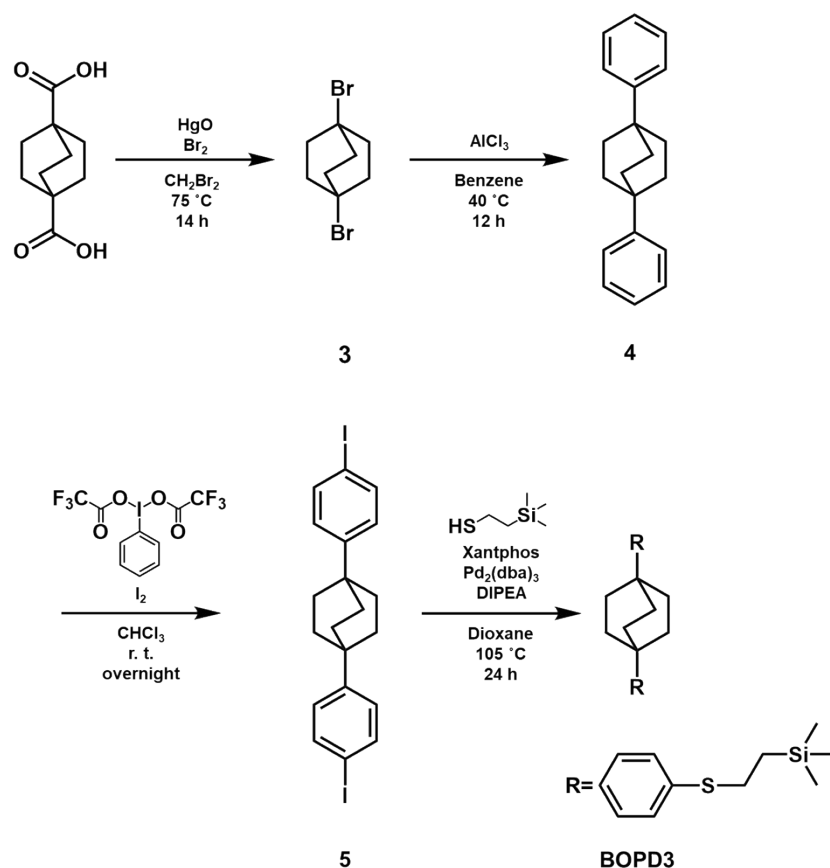
FOPD3. To a pressure tube was added 1,4-diodotetrafluorobenzene (0.05 g, 0.12 mmol, 1 equiv.), compound **2** (0.096 g, 0.29 mmol, 2.3 equiv.), and tetrakis(triphenylphosphine)palladium(0) (7.2 mg, 0.006 mmol, 0.05 equiv.). 5 mL of THF and 0.5 ml of 2M K₂CO₃ aqueous solution were added, and the mixture was purged with N₂ for 20 minutes. It was stirred at 85 °C for 72 h. It was cooled down to room temperature, saturated NaCl aqueous solution was added, and the reaction mixture was extracted with DCM 4 times. It was dried by sodium sulfate and concentrated under reduced pressure. The crude product was purified by column chromatography (Hexane : DCM = 9 : 1) to afford 48.8 mg of **FOPD3** as a white solid (yield: 69 %).

¹H NMR (400 MHz, CDCl₃) δ 7.43 (d, *J* = 8.3 Hz, 4H), 7.39 (d, *J* = 8.6 Hz, 4H), 3.07 – 3.01 (m, 4H), 1.03 – 0.97 (m, 4H), 0.08 (s, 18H).

¹³C NMR (101 MHz, CDCl₃) δ -1.59, 16.82, 28.96, 124.36, 127.31, 127.90, 129.34, 130.61, 139.71.

¹⁹F NMR (376 MHz, CDCl₃) δ -144.39.

GC-MS for [C₂₈H₃₄F₄S₂Si₂]⁺ : 566.1569 (found) 566.1571 (calcd)



1.2 Synthesis of BOPD3 (4,4'-(bicyclo[2.2.2]octane-1,4-diyl)dibenzenethiol)

Compound 3. Compound 3 was prepared following previous procedure with slight modifications.¹ To a 500 mL two-neck round bottom flask with a condenser were added bicyclo[2.2.2]octane-1,4-dicarboxylic acid (3.8 g, 19.2 mmol, 1 equiv.), red mercury(II) oxide (6.73 g, 31.1 mmol, 1.6 equiv.), MgSO₄ (4.8 g, 39.9 mmol, 2.1 equiv.) in 150 ml of dibromomethane. It was stirred vigorously at 75 °C, and Br₂ (6.40 g, 40.0 mmol, 2.1 equiv.) in 60 ml of dibromomethane was added dropwise slowly. The reaction mixture was stirred for 14 h after adding Br₂ was complete. It was cooled down to room temperature, filtered through Celite, and washed with saturated sodium bicarbonate solution 3 times. It was then washed with brine once and dried with MgSO₄. The organic layer was concentrated under reduced pressure and

purified by recrystallization with acetone to afford 2.8 g of compound **3** as a white solid (yield: 54.5 %).

^1H NMR (400 MHz, CDCl_3) δ 2.37 (s, 12H).

^{13}C NMR (101 MHz, CDCl_3) δ 40.34, 59.04.

Compound 4. Compound **3** (0.2 g, 0.75 mmol, 1 equiv.) in 20 ml of anhydrous benzene was purged for 20 minutes in 50 ml two-neck round bottom flask, and the solution was cooled to 0 °C in an ice bath. To the solution was added AlCl_3 (0.065 g, 0.49 mmol, 0.65 equiv.), and the mixture was stirred at 40 °C for 12 h under N_2 condition. The reaction mixture was quenched with ice water, extracted with chloroform 3 times, and concentrated under reduced pressure. It was purified by column chromatography (hexane : chloroform = 9 : 1) to afford 0.12 g of compound **4** as a white solid (yield: 61.0 %).

^1H NMR (400 MHz, CDCl_3) δ 7.42 – 7.36 (m, 4H), 7.33 (t, $J = 7.7$ Hz, 4H), 7.24 – 7.17 (m, 2H), 1.99 (s, 12H).

^{13}C NMR (101 MHz, CDCl_3) δ 32.93, 35.13, 125.67, 125.75, 126.07, 128.26, 149.99.

Compound 5. Compound **5** was prepared by following the previous protocol with a slight modification.² To a two-neck round bottom flask were added iodine (76.5 mg, 0.30 mmol, 1.6 equiv.) and (Bis(trifluoroacetoxy)iodo)benzene (0.17 g, 0.39 mmol, 2.1 equiv.) under N_2 condition. Compound **4** (50 mg, 0.19 mmol, 1 equiv.) in 3mL chloroform was purged with N_2 and then added to the solid mixture. It was stirred at room temperature overnight under N_2 . Saturated sodium sulfite aqueous solution was added, and the reaction mixture was extracted with chloroform 4 times. It was dried with sodium sulfate and concentrated under reduced

pressure. The crude molecules were recrystallized with chlorobenzene to afford 60.2 mg of compound **5** (yield: 61.6 %).

^1H NMR (400 MHz, CD_2Cl_2) δ 7.66 – 7.60 (m, 4H), 7.15 – 7.10 (m, 4H), 1.92 (s, 12H).

BOPD3. Compound **5** (50 mg, 0.097 mmol, 1 equiv.), Xantphos (8.2 mg, 0.014 mmol, 0.15 equiv.) and tris(dibenzylideneacetone)dipalladium(0) (9.0 mg, 0.0098 mmol, 0.1 equiv.) in 5 mL of anhydrous 1,4-dioxane were purged with N_2 for 20 minutes. *N,N*-Diisopropylethylamine (0.126 g, 0.97 mmol, 10 equiv.) and 2-(trimethylsilyl)ethanethiol (78.4 mg, 0.58 mmol, 6 equiv.) were added to the reaction mixture, and it was stirred at 105 °C for 24 h. After the reaction was complete solvent was evaporated under reduced pressure, and it was dissolved again with DCM. The reaction mixture was washed with brine three times and dried with sodium sulfate. It was concentrated under reduced pressure, and purified by column chromatography (hexane : DCM = 9:1) to afford 31.9 mg of **BOPD3** as white solid (yield= 62.4 %).

^1H NMR (400 MHz, CD_2Cl_2) δ 7.29 (d, J = 8.7 Hz, 4H), 7.24 (d, J = 8.6 Hz, 4H), 3.00 – 2.91 (m, 4H), 1.94 (s, 12H), 0.95 – 0.90 (m, 4H), 0.04 (s, 18H).

^{13}C NMR (101 MHz, CD_2Cl_2) δ -1.73, 17.35, 30.01, 33.11, 35.10, 126.50, 129.16, 134.43, 148.03.

GC-MS for $[\text{C}_{30}\text{H}_{46}\text{S}_2\text{Si}_2]^+$: 526.2557 (found) 526.2574 (calcd)

1.3 Synthesis of OPD3 (Terphenyl dithiol)

4,4''-Diiodo-*p*-terphenyl (50 mg, 0.10 mmol, 1 equiv.), Xantphos (8.7 mg, 0.015 mmol, 0.15 equiv.) and tris(dibenzylideneacetone)dipalladium(0) (9.5 mg, 0.01 mmol, 0.1 equiv.) in 5 mL of anhydrous 1,4-dioxane were purged with N_2 for 20 minutes. *N,N*-Diisopropylethylamine (0.13 g, 1.03 mmol, 10 equiv.) and 2-(trimethylsilyl)ethanethiol (8.4 mg, 0.62 mmol, 6 equiv.) were

added to the reaction mixture, and it was stirred at 105 °C for 24 h. After the reaction was complete solvent was evaporated under reduced pressure, and it was dissolved again with DCM. The reaction mixture was washed with brine three times and dried with sodium sulfate. It was concentrated under reduced pressure, and purified by column chromatography (hexane : DCM = 9:1) to afford 38.6 mg of **OPD3** as white solid (yield= 75.2 %).

$^1\text{H NMR}$ (400 MHz, CD_2Cl_2) δ 7.68 (s, 4H), 7.59 (d, $J = 8.5$ Hz, 4H), 7.38 (d, $J = 8.4$ Hz, 4H), 3.08 – 2.98 (m, 4H), 1.02 – 0.92 (m, 4H), 0.07 (s, 18H).

2. X-ray Photoelectron Spectroscopy (XPS).

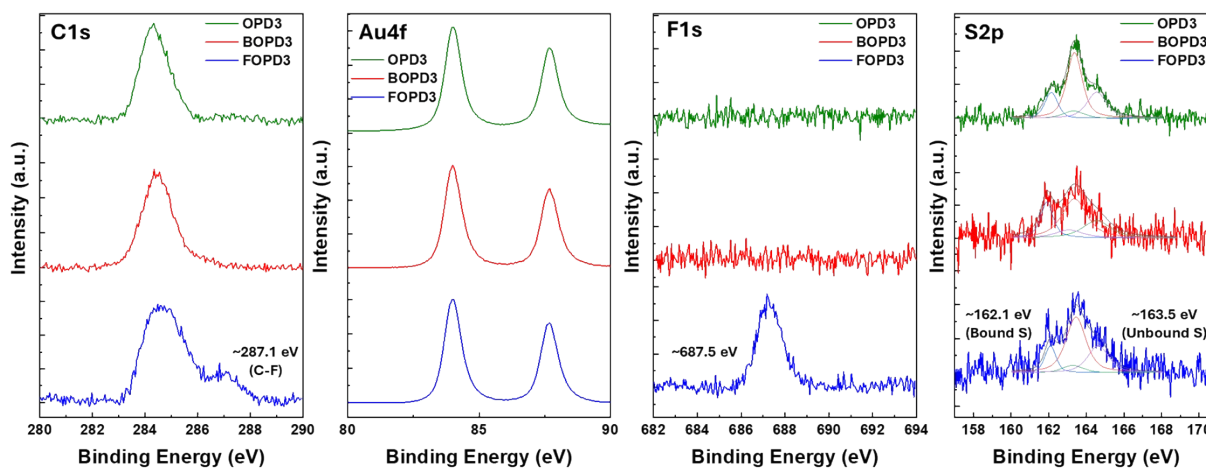


Figure S1. XPS characterization of pure OPD3, BOPD3 and FOPD3 SAMs on Au.

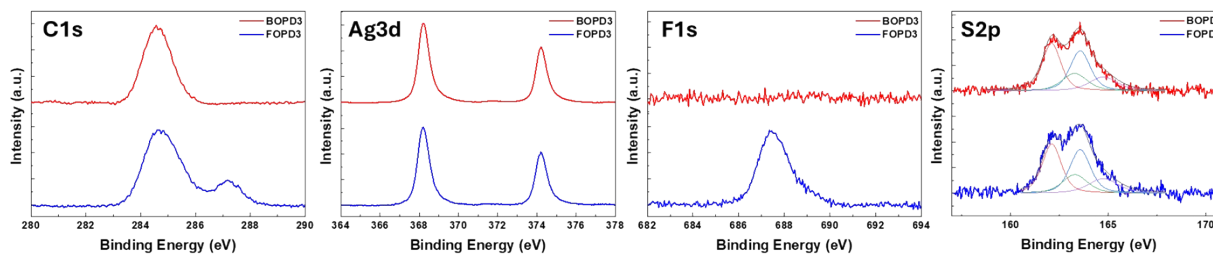


Figure S2. XPS characterization of pure BOPD3 and FOPD3 SAMs on Ag.

3. Angle Resolved XPS.

Angle-resolved XPS (ARXPS) was employed to measure the thickness of molecular layer on SAMs of different molecules. When photoelectrons come out from a sample at the specific angle α , as shown in Figure S3A, the intensity of photoelectrons can be expressed as $I = I_0 e^{-d/(\lambda \sin \alpha)}$. I_0 is the intensity of photoelectron on a bare metal substrate without molecular layer, I is the attenuated photoelectron intensity due to the SAM layer. d is the thickness of the SAM, λ is the attenuation length (4.2 nm for Au_{4f}), and α is the take-off angle between the sample and the analyzer. The thickness of the SAM layer can be obtained as a slope in the plot of $\ln|I/I_0|$ versus $1/(\lambda \sin \alpha)$. Different take-off angles (30°, 40°, 50°, 60°, and 70°) were used for the measurement of Au_{4f} photoelectron for SAMs and bare metal substrates, and the results were shown in Figure S3B. The thickness values were similar to those from ellipsometry, and they were summarized in Table S1. The molecular tilt angle was calculated based on the estimated thickness (molecular length in addition to Au-S bond length), giving 16-41° of tilt angle.

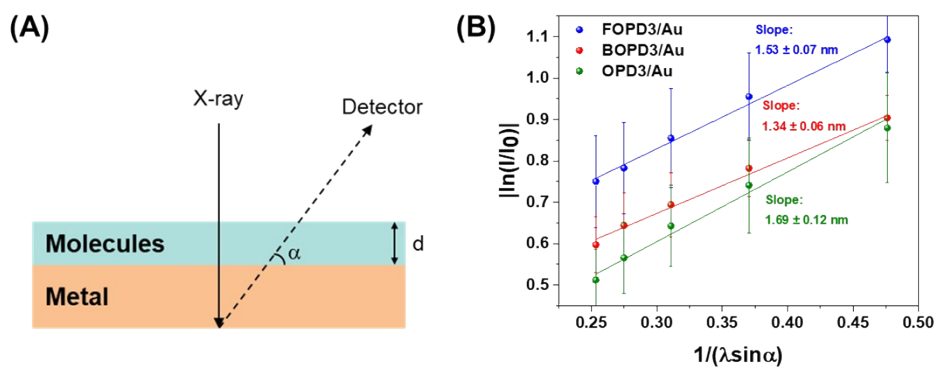


Figure S3. (A) A general description of ARXPS. (B) A plot of $\ln(I/I_0)$ vs $1/(\lambda \sin \alpha)$. Thickness was calculated from the slope of the linear fit.

Table S1. Thickness measurements by ARXPS for BOPD3, FOPD3, and OPD3 on Au. Molecular structure was optimized by Chem3D software (MM2), and the molecular length was determined as the distance between terminal H to S plus Sulfur-metal bond length (2.35 Å).

	Estimated length (nm)	ARXPS (nm)	Tilt Angle
BOPD3/Au	1.77	1.34 ± 0.06	41.0
FOPD3/Au	1.75	1.53 ± 0.07	29.3
OPD3/Au	1.76	1.69 ± 0.12	16.1

4. Ultraviolet Photoelectron Spectroscopy.

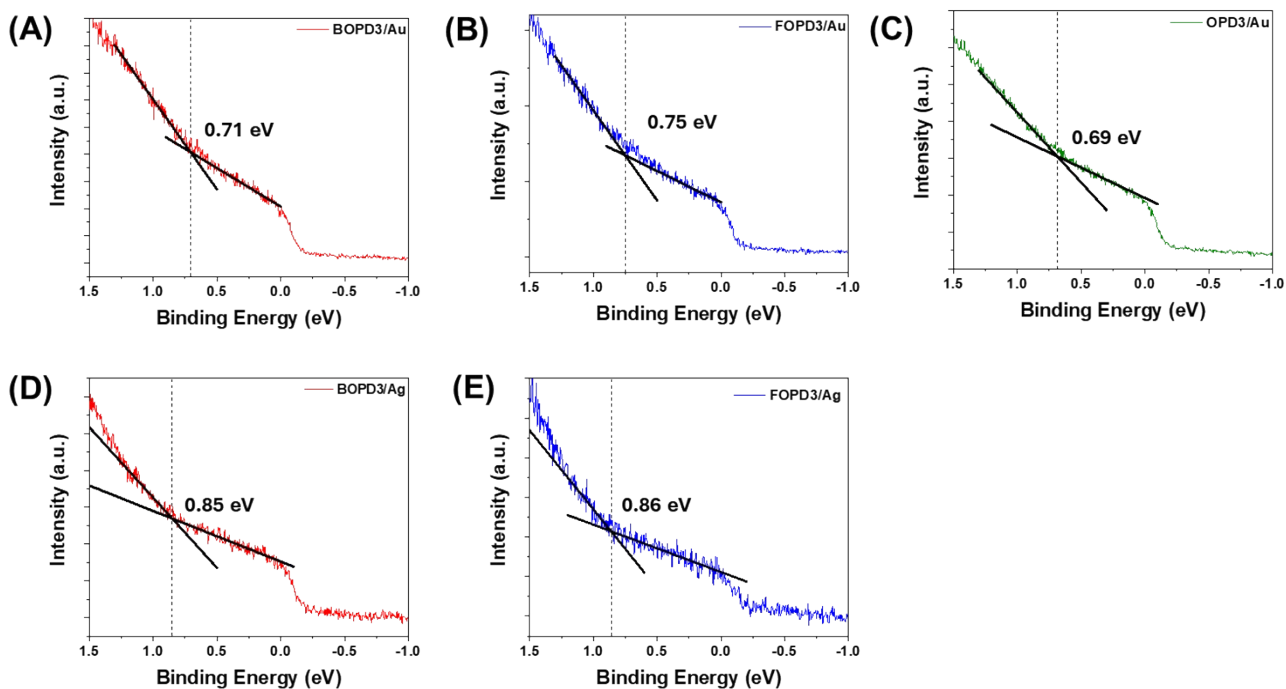


Figure S4. Measurements of the HOMO binding energy by UPS for BOPD3, FOPD3, and OPD3 SAMs on Au (A-C) and BOPD3 and FOPD3 SAMs on Ag (D-E).

5. I - V traces for Ag Junctions.

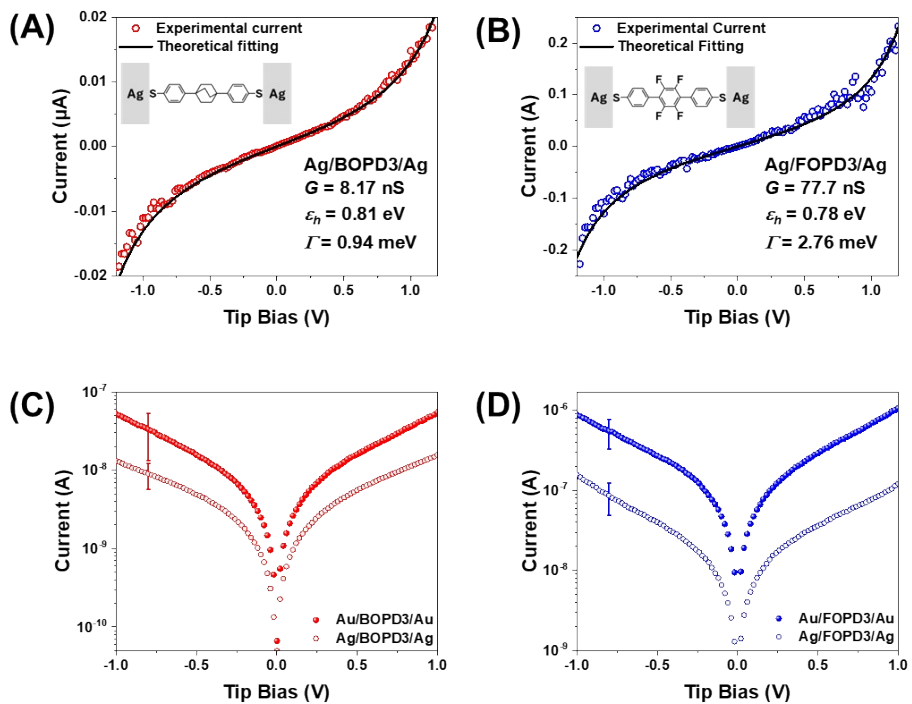


Figure S5. Individual I - V characteristics for $\text{Ag}^{\text{TS}}/\text{SAM}/\text{Ag}^{\text{Tip}}$ junctions of (A) BOPD3 and (B) FOPD3. Single level model was used to extract electronic parameters shown in the insets. (C) and (D) show semi-log plots of average I - V curves for $\text{Au}^{\text{TS}}/\text{SAM}/\text{Au}^{\text{Tip}}$ junctions and $\text{Ag}^{\text{TS}}/\text{SAM}/\text{Ag}^{\text{Tip}}$ junctions for BOPD3 and FOPD3 SAMs, respectively.

6. Fit to the Non-Dimensionalized Prediction for Off-Resonance Tunneling (I_R vs V_R).

Non-dimensional parameters for current and voltage, denoted as I_R and V_R , are defined as $I_R = I / I_C$ and $V_R = V / V_C$, respectively, as shown in Figure S6. Characteristic voltage (V_C) and current (I_C) are transition points where the I - V curve shifts from an ohmic linear regime ($V < V_C$) to a non-linear regime ($V > V_C$). Consistent with prior studies^{3,4}, V_C is obtained as the maximum value in the recast dataset of $|V^2/I|$ plotted against V , Figure S6B. Substituting V_C , identified as the maximum of $|V^2/I|$ vs V , into equation 1 allows V_C and I_C to be expressed as:

$$\frac{\partial}{\partial V} \left(\frac{V^2}{I} \right)_{V=V_C} = 0 \quad (\text{S1})$$

$$eV_C = 2|\varepsilon_0|/\sqrt{3} \quad (\text{S2})$$

$$I_C = \sqrt{3} G |\varepsilon_0|/e \quad (\text{S3})$$

Using equations S1, S2 and the definition of I_R and V_R , equation 1 can be reformulated in terms of the non-dimensional parameters V_R and I_R , as shown in equation 3.

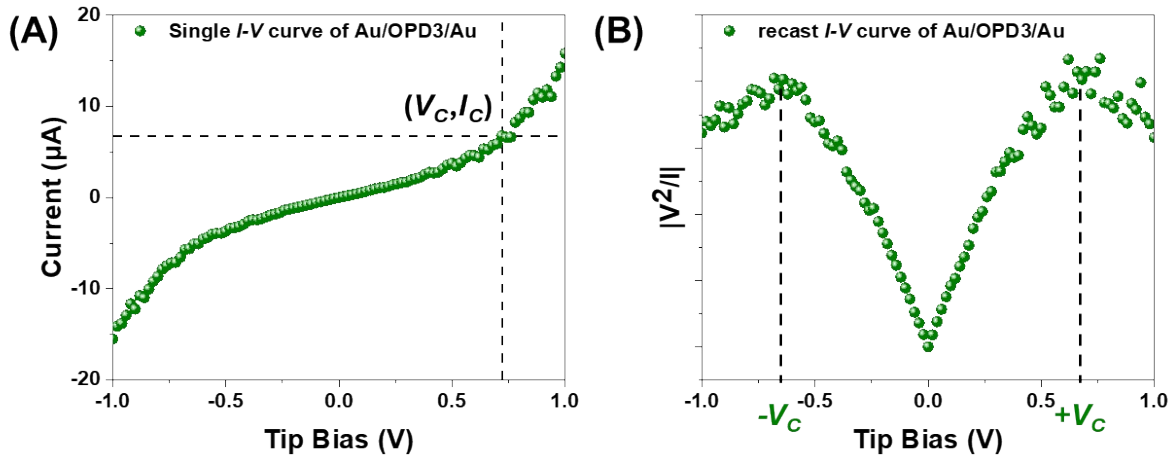


Figure S6. (A) Representative single I - V characteristic of an $\text{Au}^{\text{TS}}/\text{OPD3}/\text{Au}^{\text{Tip}}$ junction. (B) The corresponding plot of $|V^2/I|$ vs V , where the maximum value is used to define V_C and corresponding I_C . These values are utilized for non-dimensional I_R - V_R analysis, which demonstrates strong alignment with the theoretical I_R vs V_R prediction for off-resonant tunneling.

7. Current-Voltage Behavior of Binary Component SAMs.

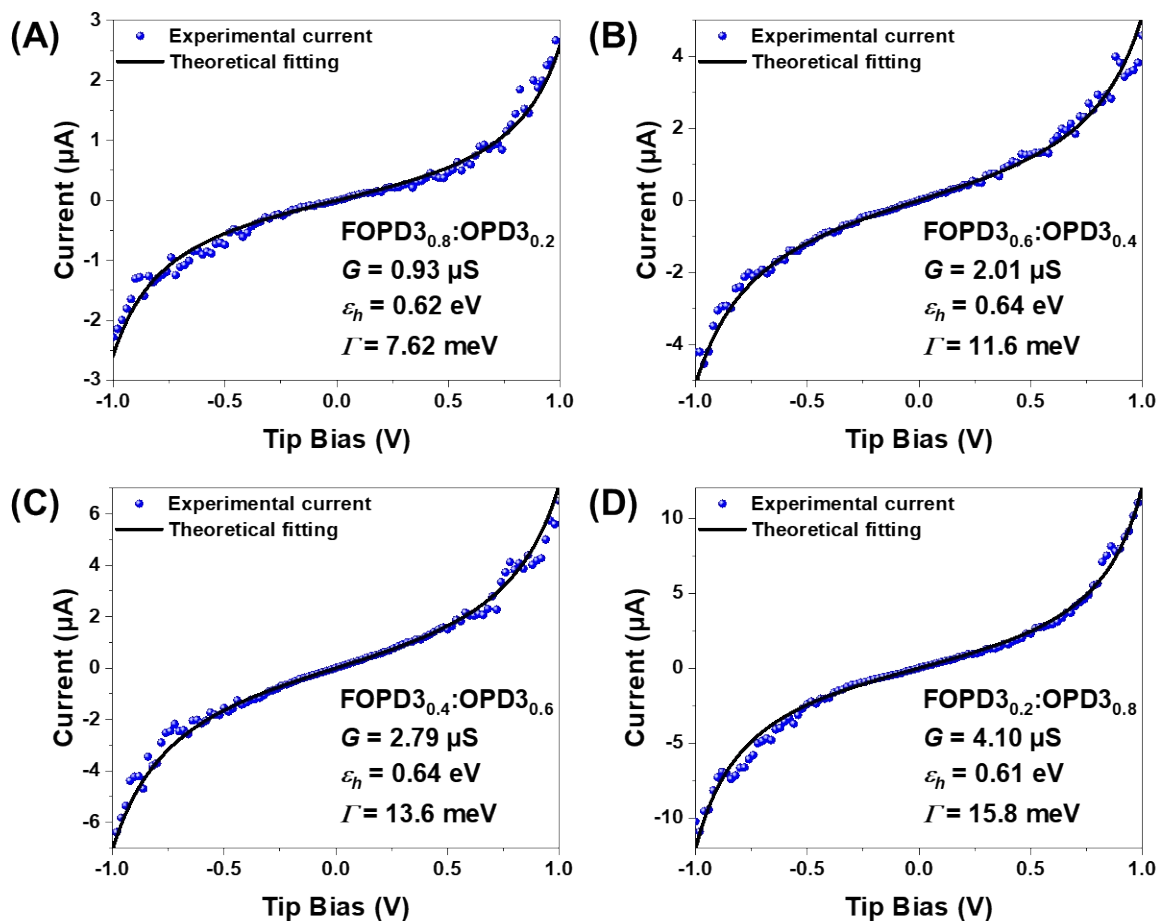


Figure S7. Current-voltage behavior of FOPD3_x:OPD3_(1-x) mixed SAMs. (A-D) Representative individual I - V characteristics of $\text{Au}^{\text{TS}}/\text{SAM}/\text{Au}^{\text{Tip}}$ junctions for FOPD3_x:OPD3_(1-x) SAMs. Pure FOPD3 and OPD3 data were shown in Figure 2. Black lines are two parameter fits to the off-resonance single level model (or-SLM). Fit parameters G and ε_h are shown in the insets, as well as metal-HOMO coupling Γ calculated from equation 2 using $N \cong 80$.

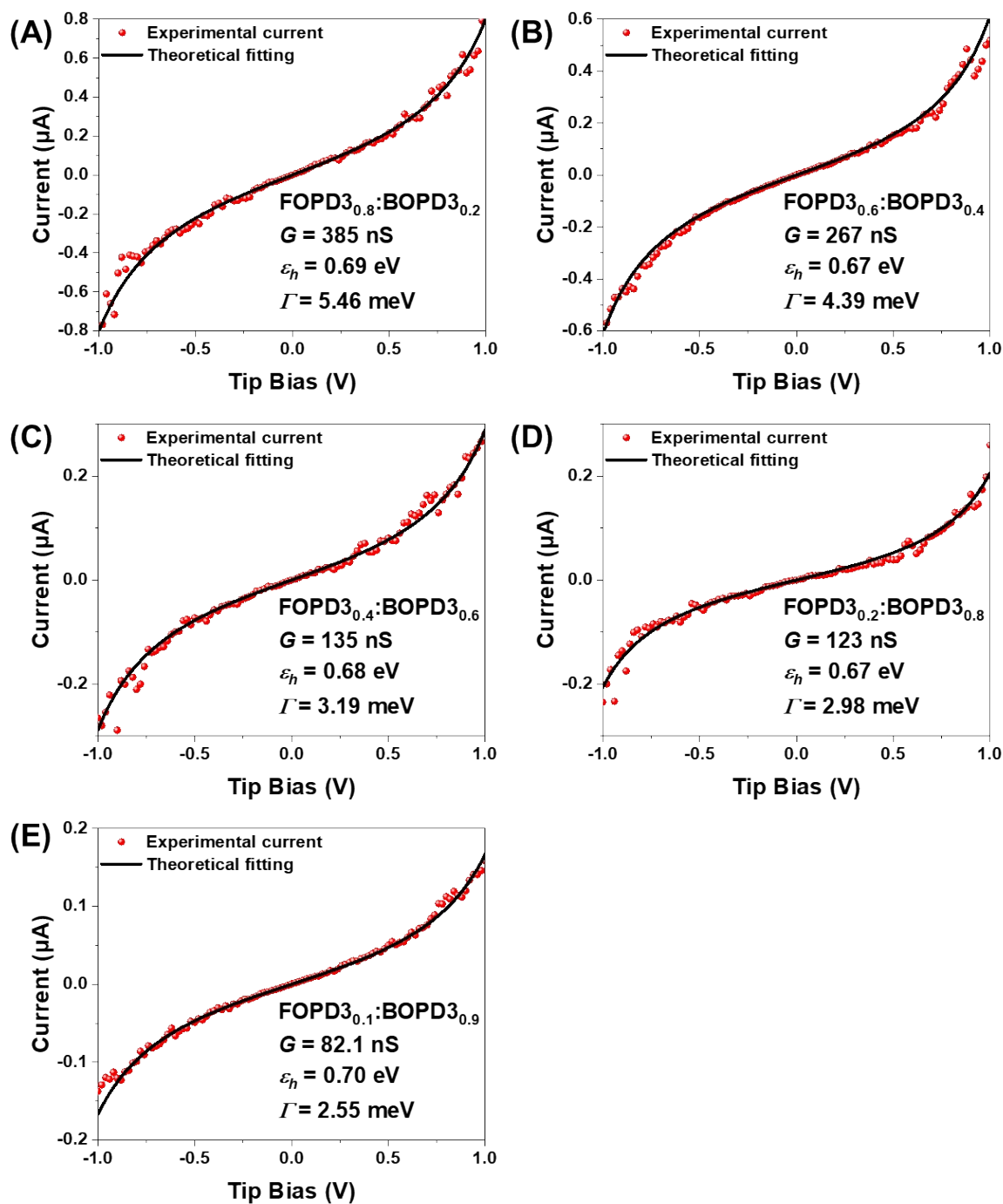


Figure S8. Current-voltage behavior of FOPD3_x:BOPD3_(1-x) mixed SAMs. (A-E) Representative individual I - V characteristics of $\text{Au}^{\text{TS}}/\text{SAM}/\text{Au}^{\text{TP}}$ junctions for FOPD3_x:BOPD3_(1-x) SAMs. Pure FOPD3 and BOPD3 data were shown in Figure 2. Black lines are two parameter fits to the off-resonance single level model (or-SLM). Fit parameters G and ϵ_h are shown in the insets, as well as metal-HOMO coupling Γ calculated from equation 2 using $N \cong 80$.

8. Single Level Model Analysis with Mixed SAM Composition.

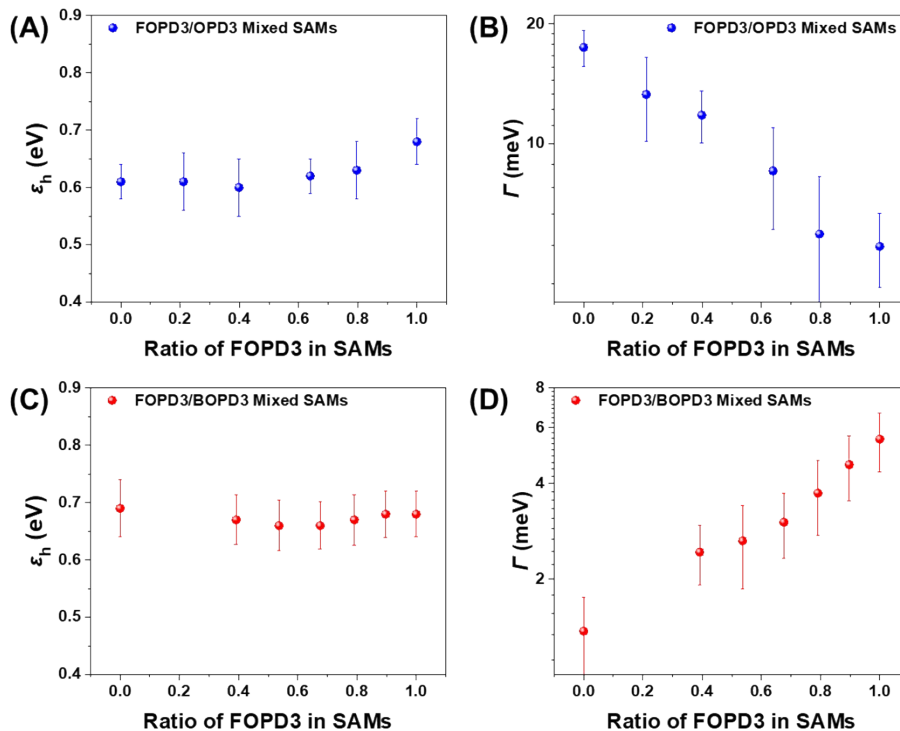


Figure S9. Junction electronic structure parameters versus binary SAM composition. (A) ϵ_h versus SAM composition and (B) semilog plot of Γ versus SAM composition for FOPD3_x:OPD3_(1-x) mixed junctions. (C) ϵ_h versus SAM composition and (D) semilog plot of Γ versus SAM composition for FOPD3_x:BOPD3_(1-x) mixed junctions. In all cases ϵ_h and Γ were extracted from I - V characteristics using the orSLM.

9. Density Functional Calculations of HOMO for BOPD3, FOPD3, and OPD3.

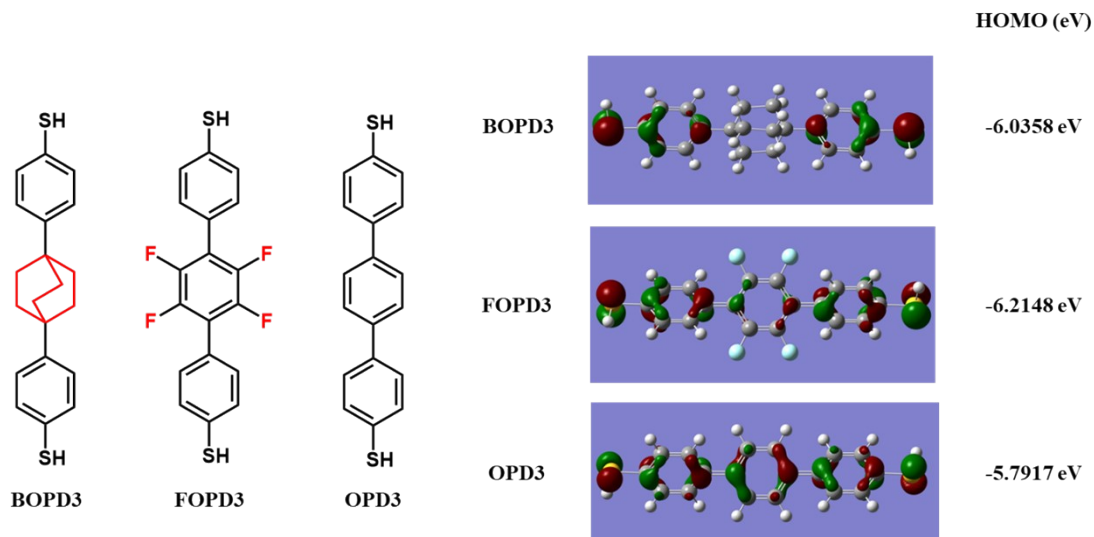


Figure S10. Results of HOMO calculation of BOPD3, FOPD3, OPD3 molecules by Gaussian 16 software with 6-311++g(d,p) basis sets.⁵

References

- 1 K. B. Wiberg, W. E. Pratt and W. F. Bailey, *J. Am. Chem. Soc.*, 1977, **99**, 2297–2302.
- 2 H. Langhals, P. Braun, C. Dietl and P. Mayer, *Chemistry A European J*, 2013, **19**, 13511–13521.
- 3 Z. Xie, I. Bâldea, S. Oram, C. E. Smith and C. D. Frisbie, *ACS Nano*, 2017, **11**, 569–578.
- 4 I. Bâldea, Z. Xie and C. D. Frisbie, *Nanoscale*, 2015, **7**, 10465–10471.
- 5 Gaussian 16, Revision B.01, Frisch, M. J.; Trucks, G. W.; Schlegel, H. B.; Scuseria, G. E.; Robb, M. A.; Cheeseman, J. R.; Scalmani, G.; Barone, V.; Petersson, G. A.; Nakatsuji, H.; Li, X.; Caricato, M.; Marenich, A. V.; Bloino, J.; Janesko, B. G.; Gomperts, R.; Mennucci, B.; Hratchian, H. P.; Ortiz, J. V.; Izmaylov, A. F.; Sonnenberg, J. L.; Williams-Young, D.; Ding, F.; Lipparini, F.; Egidi, F.; Goings, J.; Peng, B.; Petrone, A.; Henderson, T.; Ranasinghe, D.; Zakrzewski, V. G.; Gao, J.; Rega, N.; Zheng, G.; Liang, W.; Hada, M.; Ehara, M.; Toyota, K.; Fukuda, R.; Hasegawa, J.; Ishida, M.; Nakajima, T.; Honda, Y.; Kitao, O.; Nakai, H.; Vreven, T.; Throssell, K.; Montgomery, J. A., Jr.; Peralta, J. E.; Ogliaro, F.; Bearpark, M. J.; Heyd, J. J.; Brothers, E. N.; Kudin, K. N.; Staroverov, V. N.; Keith, T. A.; Kobayashi, R.; Normand, J.; Raghavachari, K.; Rendell, A. P.; Burant, J. C.; Iyengar, S. S.; Tomasi, J.; Cossi, M.; Millam, J. M.; Klene, M.; Adamo, C.; Cammi, R.; Ochterski, J. W.; Martin, R. L.; Morokuma, K.; Farkas, O.; Foresman, J. B.; Fox, D. J. *Gaussian, Inc., Wallingford CT*, **2016**.